2020-01-1618 Published 05 Oct 2020



Transient Heat Transfer Simulation and Buckling Analysis of Disc Brakes in In-Wheel Motor-Driven Vehicles

Kingsford Koranteng, Joseph-shaahu Shaahu, and Yun-Bo Yi University of Denver

Citation: Koranteng, K., Shaahu, J.-S., and Yi, Y.-B., "Transient Heat Transfer Simulation and Buckling Analysis of Disc Brakes in In-Wheel Motor-Driven Vehicles," SAE Technical Paper 2020-01-1618, 2020, doi:10.4271/2020-01-1618.

Abstract

igh-temperature distributions in disc brake mounted within in-wheel motor-driven vehicles have several negative effects on braking performance. This is mainly due to the enclosed nature of the brake components. This paper aims to determine the effect of contact geometry on temperature distribution and thermal buckling in such a brake. Numerical analysis is conducted to investigate the variation of temperature field on the brake disc at different cover angles of pads while maintaining the same moment of friction. The effect of different radial positions of the pads is a second consideration in the current work, using a transient

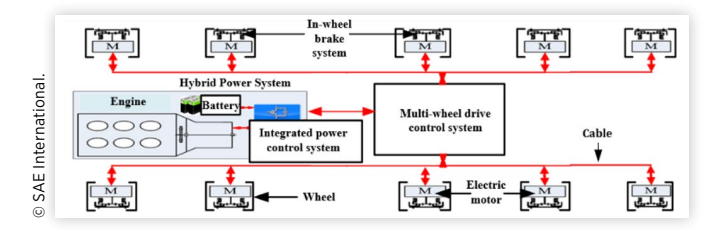
modeling approach. To validate the simulation results, an approximate, analytical solution is derived according to energy conservation. The results show that, for the same work done by the pads, the maximum temperature on the disc increases with a decrease in the pad cover angle. Also, the pad positions were found to affect temperature distribution significantly on the friction disc surface. More importantly, the effect of the resulting temperature distribution on thermal buckling of the disc is also considered. It was found that, for the same friction work, certain contact geometry can cause the braking temperature to exceed the critical thermal buckling temperature, leading to buckling during brake operations.

1. Introduction

here are increasing demands and research on in-wheel motor-driven vehicles for both hybrid and fully electric vehicles due to several advantages provided by this technology [1]. The innovation makes it easier to develop simple intelligent brakes with an appropriate control strategy for the anti-lock brake system and it has the potential to create an all-wheel-drive [2]. More importantly, this technology provides the opportunity to independently control the steering and speed of individual wheels since each wheel is driven by an electric motor as seen in Fig 1.

Besides, because the brake components are mounted within the wheels, the brake system is referred to as an in-wheel brake system. Despite these advantages, a major challenge with this technology is the design of the disc brake system, which is usually mounted within the wheels. The space available inside the wheels for the design of the disc brake components is limited, even in the case of heavy vehicles.

FIGURE 1 Schematics of an in-wheel motor-driven vehicle

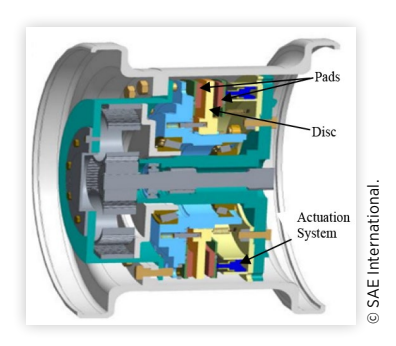


This makes it difficult to design appropriate disc brake components which can minimize the onset of thermal buckling and thermoelastic instability during braking. The enclosed nature of the brake system makes it even more difficult to control heat resulting from braking. Therefore, heat is not effectively and efficiently dissipated quickly from the sliding components to the outside environment. This can lead to the damage of the electric motor and also onset thermo-mechanical instability during braking as a result of a high rise in temperature.

In this paper, a disc brake system designed for a 10×10 multi- in- wheeled motor-driven vehicle is studied during braking at full vehicle load. The main objective is to investigate the influence of different cover angles of the pads and the pad positions on temperature field distribution. Also, to investigate the effect of the resulting temperature field on thermal buckling during braking. At present, there are few works on the brake system of an in-wheeled vehicle that considers the full vehicle dynamics and the effect of contact geometry on temperature field distribution and thermal buckling. Moreover, due to the high torque demands of the reference vehicle, each wheel is designed to have four brake pads mounted within it. Each side of the rotor has two brake pads of the same parameters and alignments which is pressed against the rotor upon brake application. In order to decide on the appropriate positions and cover angles of the pad for the 10X10 multi- in- wheeled vehicle brake system, a fully coupled temperature displacement analysis is performed using ABAQUS. Thermal stresses and thermal expansion resulting

FIGURE 2 Completed structure of the in-wheel

brake system



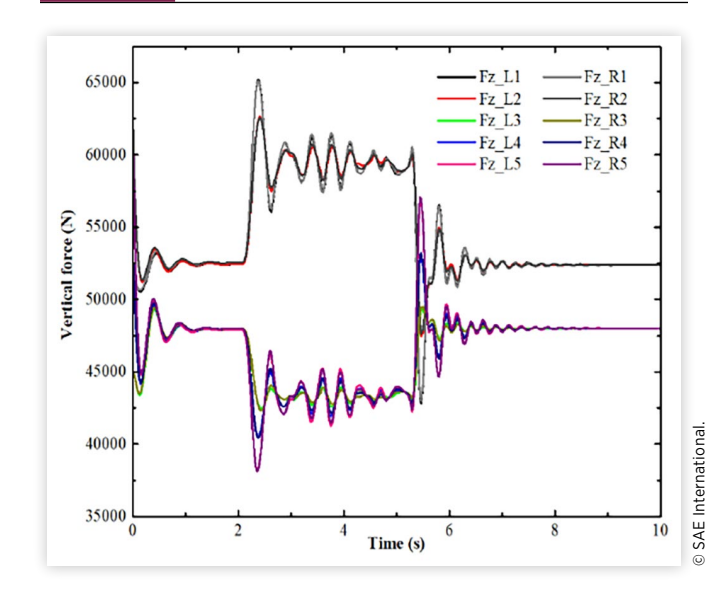
from braking were not considered in the heat analysis but were considered in the thermal buckling analysis. The brake system of the reference vehicle comprised of a rotor disc that can move axially, a fixed brake pad, and at least one axially moving brake pad provided on each side of the rotor disc (<u>Fig.2</u>). Frictional heat is produced when the fixed and axially moving pad is clamped against the rotating disc. The generated frictional heat can cause several negative effects on the brake system such as thermal buckling, thermal cracks, thermal hot spots, brake fade and also damage to the electric motor due to the enclosed nature of the brake components [3, 4, 5, 6]. Therefore, it is very crucial to carry out thermal analysis to predict the effect of the resulting temperature distribution on the brake components during braking [7, 8]. Research has shown that non-uniform temperature distribution in brake disc influences thermal buckling, which in turn promotes thermoelastic instability [9, 10]. Chen et al. [9] carried out a numerical study on the coupling between thermoelastic instability and thermal buckling in clutches. They discovered that unstable temperature modes induced by thermoelastic instability can change the temperature profiles for thermal buckling. Furthermore, a Fourier finite element model developed by Chen et al. [11] for identifying thermal buckling in disc clutches and brakes revealed that there is a specific wave number with which the buckling temperature approaches a minimum value. Therefore, it is very important to predict the thermal buckling phenomenon of brakes during the design stage in order to prevent uncertainties in brakes performance [12]. Moreover, at high sliding speed, the temperature of the disc rotor becomes unstable leading to high temperature at localized regions known as hot spots on the sliding interface [13, 14]. This hot spot appears on the contact surface of the disc as a result of thermoelastic instability (TEI) caused by thermal buckling [10, 15]. Lee & Barber [16] studied the thermoelastic instability in the disc brake system and found that the onset of instability is always characterized by an antisymmetric perturbation. The energy generated at the interface of the pad and rotor during braking is transferred into the two bodies [17, 18]. As a result, the rotor which absorbs most of the heat must be designed to effectively and efficiently dissipate the absorbed heat. Due to the high cost of conducting experimental studies on temperature field, numerical methods and analytical methods are widely used by researchers to obtain appropriate results before proceeding to the production phase of the disc brake [19, 20]. Talati and Jalalifar [18] conducted a study on the heat conduction in a disc brake system using an analytical approach. A microscopic model was used to investigate the heat generation and the results showed that there is heat partition during sliding due to thermal resistance. Furthermore, several research works have proven that numerical simulations correlate best with experimental results than the analytical approach. This was observed in a study conducted by Yevtushenko et al. [20]. The braking performance of a vehicle is greatly influenced by temperature distributions in the brake components. Therefore, it is important to predict the temperature rise in the brake components at the early stages, in order to design appropriate brake components.

2. Thermal Analysis of the **Disk Rotor and Pad Contact**

The temperature distribution field and buckling analysis are carried out on a three-dimensional axisymmetric rotor of the 10X10 in-wheeled vehicle brake system. The total vertical loads $F_z(L, R)$ acting on each wheel during braking are obtained by performing dynamic simulation using TRUCK SIM (Fig.3).

For analysis purposes, the first right wheel $(F_z R1)$ of the reference vehicle is considered due to the highest vertical force exhibited during braking. Braking was applied to the vehicle moving with an initial velocity of 30 km/h at t = 4.2 s and the dynamic loads acting on the vehicle wheels are observed. From the resulting forces, the required parameters needed to carry out the numerical studies were computed. The disc brake which is subjected to high axisymmetric thermal load may result in non-uniform temperature distribution in the rotor. The influence of contact geometry and the resulting temperature field effect on thermal buckling of the disc are investigated.

Vertical load acting on each wheel of the vehicle



3. Analytical Model

During brake application, the vehicle starts to decelerate from its initial velocity to a final velocity. The energy of the vehicle during this process is expressed in <u>Eq. (1)</u>.

$$E_b = \frac{1}{2} \left\lceil M \left(v_i^2 - v_f^2 \right) + I \left(\omega_i^2 - \omega_f^2 \right) \right\rceil \tag{1}$$

When the driver completely brings the vehicle to rest, the final velocity and angular velocity becomes zero and Eq. (1) becomes:

$$E_B = \frac{1}{2} \left[M(v_i^2) + I(\omega_i^2) \right]$$
 (2)

The decelerating power of the brake is obtained by finding the derivative of the vehicle kinetic energy during braking as expressed below:

$$P_{d} = \frac{d}{dt} \left(\frac{Mv^{2}}{2} \right) = M \frac{dv}{dt} = MR^{2} \omega(t) \alpha_{t}$$
 (3)

Where

$$\omega(t) = \omega_o + \alpha_t t$$

Here, α_t represents the angular acceleration and v represents the velocity of the vehicle. Also, it was assumed that the brake decelerating power is equivalent to the total friction heat during braking.

$$P_d = P_f$$

Moreover, since the whole vehicle has forty brake pads, the friction heat rate can be expressed by the integral below:

$$P_f = 40 \iint (f_f \cdot v) dA_p = (-40) f_f(t) \iint r dA_p \tag{4}$$

Equations 3 and 4 can be combined to obtain the total friction force f_f generated by the vehicle during braking:

$$f_f = \frac{MR^2 \alpha_t}{40r_{tt} Ap} \tag{5}$$

From Eq. (5), the total heat generated by the vehicle is obtained by finding the dot product of the vehicle velocity and the friction force.

$$q(r,t) = \gamma \cdot f_f \cdot \nu(t) = \gamma \left(\frac{MR^2 \alpha}{40 r_m A p} \cdot r(\omega_o + \alpha_t t) \right)$$
 (6)

Where, γ is the heat partition coefficient.

Also, by considering the following conditions: Weight distribution on all the four front wheels =0.59; Only one front brake rotor is considered=1/4; Only one side of the rotor is considered=0.5.

The heat flux on one side of a single rotor for a single front wheel can be computed as:

$$q(r,t) = \dot{Q}_{in} = \gamma \cdot f_f \cdot v(t) = (0.59) \frac{1}{4} (0.5) \gamma \left(\frac{MR^2 \alpha_t}{40 r_e A p} r(\omega_o + \alpha_t t) \right)$$
(7)

The equilibrium equation for the heat generated can be expressed as:

$$C_{p}.m_{d}.\frac{dT}{dt} = \dot{Q}_{in} (Q_{brake_heat}) - \dot{Q}_{out} (Q_{conduction} - Q_{convection}) (8)$$

$$C_p m_d \frac{dT}{dt} = \dot{Q}_{in} - K_d A_d (T_s - T_a) - h A_s (T_s - T_a)$$
 (9)

To estimate the heat transfer coefficient, Reynold's number [21] was computed using Eq. (10).

$$Re = \frac{\omega r^2}{v} < 2.4 \times 10^5$$
 (10)

Also, knowing Reynold's number $Re < 2.4 \times 10^5$, the heat transfer coefficient for the disc having a laminar flow [22, 23] is computed from Eq. 11.

$$h = 0.70 \left(\frac{K_a}{D}\right) \text{Re}^{0.55}$$
 (11)

Combining these equations, an expression for the change in temperature within the disc during braking is obtained. A Simulink model is developed based on this expression to compute the change in temperature.

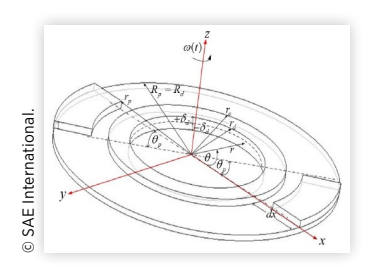
$$\frac{dT}{dt} = -\frac{K_d A_d T_s}{C_p m_d} - \frac{h A_s T_s}{C_p m_d} + \frac{(0.59) \frac{1}{4} (0.5) \gamma \left(\frac{M R^2 \alpha}{40 r_e A p} r(\omega_o + \alpha_t t)\right) + K_d A_d T_a + h A_s T_a}{C_p m_d}$$
(12)

3.1. Numerical Modeling

<u>Figure. 2</u> shows the complete structure of the in-wheeled-mounted disc brake system. In this analysis, only the pad and brake disc were considered in the finite element analysis due to the high cost of computing the complete structure [24].

Moreover, since both the disc and pads are symmetric, only half of the sections were considered, and the variables used for the boundary conditions are defined as shown in Fig.4. The disc and the annular pads have an inner radius: $r_p = 112mm$ and $r_p = 173.5mm$ respectively, and outer radius $r_p = 232mm$ and $r_p = 237mm$ respectively. The friction ring section and the pad are 5mm and 10mm in thickness respectively. The radial distance of the friction ring section which is from the outer radius (R_0) of the disc hub to the outer radius of the disc R_d is dx = 90mm. A coupled temperature-displacement analysis was carried out using ABAQUS dynamic temp-disp explicit scheme to determine the influence of pad cover angle (θ_p) and its positions on the temperature field distribution by ensuring the same moment of friction irrespective of the change in geometry or position. The 3-D model of the disc and pad are modeled in ABAQUS using an 8-node thermally coupled brick, trilinear

FIGURE 4 Geometry of the brake disc and pad



displacement and temperature, reduced integration, hourglass control element (C3D8RT element) <u>Fig. 5</u>. Surface to surface contact is defined for the friction between the element faces in the contact region. Due to the enclosed structure of the in-wheeled-mounted disc brake system, thermal radiation was not taken into consideration. The average convection heat coefficient was computed for the disc ($h = 5W/m^2/$ °C) to define the convection boundary conditions.

<u>Tables 1 & 2</u> show the material properties and parameters used in the simulation process. It was assumed that all friction resulting from the braking process is dissipated as heat. The heat flux generated at the contact interface Z=0 enters the pad and the disc respectively according to the equations below:

$$q_{p}(r,\theta,0,t) = \gamma f_{f} p\omega(t) r,$$

$$r_{p} \le r \le R_{p}, 0 \le \theta \le \theta_{p}, 0 \le t \le t,$$
(13)

$$q_d(r,\theta,0,t) = (1-\gamma) f_f p\omega(t) r,$$

$$r_p \le r \le R_p, 0 \le \theta \le 2\pi, 0 \le t \le t_s$$
(14)

Where γ is the heat partition ratio [18, 25, 26] calculated as:

$$\gamma = \frac{K_p \sqrt{\alpha_d}}{K_p \sqrt{\alpha_d} + K_d \sqrt{\alpha_p}} \tag{15}$$

FIGURE 5 3-D mesh of the brake disc and pads



TABLE 1 Parameters & thermoelastic properties used in the simulation

Dimension	Disc (65Mn)	Pad	
Elastic modulus, E _{p,d} GPa	211	100	
Poisson's ratio, $oldsymbol{v}$	0.288	0.25	
Thermal conductivity, K,W/m²°C	48	0.5	
Specific heat, C _{p,d} , J / K ° C	450	1000	
Mass density, $ ho_{ m p,d}$, (Kg/m³)	7820	1400	
Mass of the brake disc $\mathbf{m_d}$, \mathbf{kg}	2.0		
Initial Velocity V _{o,} km/h	30		
Vehicle mass M,kg	50,000		

TABLE 2 Dimensions and application parameters

Dimension	Disc (65Mn steel)	Pad
Inner radius $r_{p,d,m}$	0.112	0.173
Initial outer radius, $R_{p,d}$, m	0.237	0.232
Hub Outer radius r_0 , m	0.147	
Friction ring thickness $\delta_{p,d}$ $m{m}$	0.005	0.010
Thickness (hub portion) δ_{d} $m{m}$	0.025	
Effective radius, $re_{p,d}$ m	0.340	0.374
Wheel radius R,m	0.6	

Here, K is the thermal conductivity, α is the thermal diffusivity and the subscripts p and d represent pad and disc respectively. The governing equations for the three-dimensional temperature fields $T=(r,\theta,z,t)$ of the pad and disc are presented as follows.

Considering the disc:

$$K_{d}\left(\frac{\partial^{2}T}{\partial r^{2}} + \frac{1}{r}\frac{\partial T}{\partial r} + \frac{1}{r^{2}}\frac{\partial^{2}T}{\partial \theta^{2}} + \frac{\partial^{2}T}{\partial z^{2}}\right) = \rho c_{p}\left[\frac{\partial T}{\partial t} + \frac{V(t)}{R}\frac{\partial T}{\partial \theta}\right],$$

$$r_{d} < r < R_{d}, 0 < \theta < 2\pi, -\delta_{d} < z < 0, t < 0 < t_{s},$$

$$r_{d} < r < r_{o}, 0 < \theta < 2\pi, 0 < z < +\delta_{d}, t < 0 < t_{s}$$

$$(16)$$

Considering a single Pad:

$$K_{p}\left(\frac{\partial^{2}T}{\partial r^{2}} + \frac{1}{r}\frac{\partial T}{\partial r} + \frac{1}{r^{2}}\frac{\partial^{2}T}{\partial \theta^{2}} + \frac{\partial^{2}T}{\partial z^{2}}\right) = \rho c_{p}\frac{\partial T}{\partial t},$$

$$r_{p} \leq r \leq R_{p}, 0 \leq \theta_{p}, 0 < z < \delta_{p}, 0 < t < t_{s}$$
(17)

The boundary conditions for a single pad and disc rotor were considered, and the following initial boundary conditions were assumed:

First, taking the pad and the disc to be at ambient temperature. The boundary conditions are defined as:

$$T(r,\theta,z,0) = T_a, r_p \le r \le R_p, \tag{18}$$

$$T(r,\theta,z,0) = T_a, r_d \le r \le R_d, 0 \le \theta \le 2\pi, -\delta_p \le z \le 0$$
 (19)

$$T(r,\theta,z,0) = T_a, r_d \le r \le r_0, 0 \le \theta \le 2\pi, 0 \le z \le +\delta_d$$
 (20)

Also, the initial boundary condition for the contact region is defined as:

$$K_d \frac{\partial T}{\partial z}\Big|_{z=0^-} - K_p \frac{\partial T}{\partial z}\Big|_{z=0^+} = q(r,\theta,0,t), (r,\theta) \in A_s, 0 \le t \le t_s \quad (21)$$

Considering the initial contact surface between the pad and the brake disc, the boundary condition can be expressed as:

$$T(r,\theta,0^+,t) = T(r,\theta,0^-,t), (r,\theta) \in A_d, 0 \le t \le t_s$$
 (22)

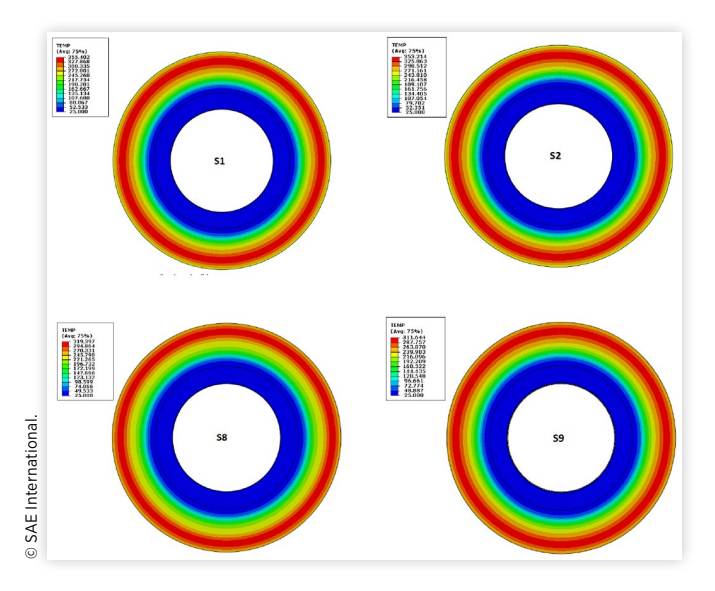
In this study, convection boundary conditions for the disc were defined for all the free surface area of the disc.

4. Simulation Results

4.1. Influence of the Cover Pad Angle θ_p on Temperature Distribution

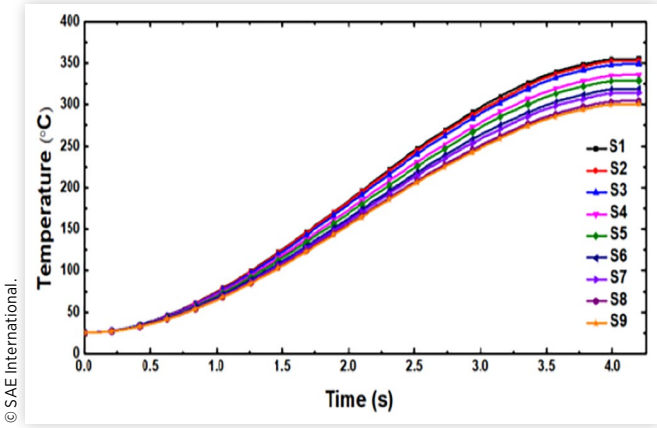
The simulation was carried out for single braking at t_s =4.2s for the vehicle decelerating with an initial velocity of 30km/h to standstill. The discs were labeled S1, S2, S3, S4, S5, S6, S7, S8 and S9 with corresponding pad cover angles (θ_p): 20°, 30°, 40°, 50°, 60°, 70°, 80°, 90° and 100° respectively. Where the pad cover angle θ_p is the size of the pad in the circumferential

FIGURE 6 Variation of temperature field on the disc at pads cover angles θ_0 of 20°,30°,90° and 100°



direction. It is quite clear that increasing the cover angle of the pad will increase the area of the pad which in turn increases the force applied on the rotor, resulting in a difference in the moment of friction. Therefore, the corresponding applied pressures for each cover angle of the pad θ_p to produce the same moment of friction or work done were computed. This approach was also used by Grześ [27]. Figure 6 shows the temperature field distribution on the disc at the various cover angles of the pads. The temperature field distributions on the discs are non-uniform as expected but appeared to have a similar distribution pattern. The red zone of the temperature distribution appeared close to the circumferential region of each disc. This could be attributed to velocity being maximum at the circumferential region. Velocity increases along disc radial to the circumferential region of the disc, hence the expected results. The similarity in the temperature field distribution pattern was because the friction force generated between each pad and the disc is the same. However, the maximum temperature values of the distributions appeared to be different. The highest maximum temperatures obtained were in the order of discs with decreasing pads cover angles. Disc S1 showed the highest maximum temperature $T_{max} = 355.40$ °C at the end of the $t_s = 4.2$ s of braking whereas disc S9 showed the lowest maximum temperature $T_{max} = 311.64$ °C. This means that, for the same work done, braking with a small pad area will lead to high-temperature distributions at localized areas on the disc. Meanwhile, braking with a larger brake pad such as S9 will increase the unsprung mass of the reference vehicle. From Fig. 7, the temperatures of the discs have a great relationship with the cover angle of the pads. The increasing trend of temperature with time for each disc was observed to have a similar profile pattern. However, the order of increasing value of temperature with time differs from each disc, with the highest being the disc with the smallest pad cover angle. Moreover, since the angular velocity of the disc is higher at the earlier stage of the braking process, the temperature rises faster in all the discs at the early stage, and then slows its rise at the latter stage of

FIGURE 7 Variation of maximum temperature with time at different cover angles of the pads

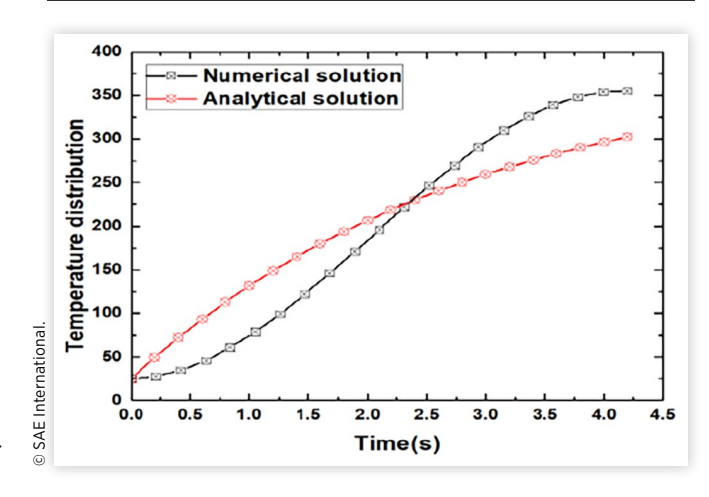


the braking process. It then decreases slightly downward when the disc was brought to a standstill due to the convection heat transfer defined. The resulting difference in the maximum temperature field distribution from S1 to S9 may also be attributed to the heat partition ratio. This is because the heat partition coefficient depends strongly on the geometry of the pads [28].

In order to verify these simulation results, a comparison with an analytical model was considered. The numerical and analytical solutions are not well correlated as there were several assumptions made like different heat transfer coefficients, boundary conditions etc. Moreover, the FEA analysis assumes more realistic modeling of the component geometry, material properties and boundary conditions [29]. Therefore, the expected qualitative and quantitative differences. For example, comparing the analytical and numerical results for braking with the pad cover angle of 30° as shown in Fig. 8, the evolution of temperature for the analytical and the numerical simulation begins at room temperature of 25°C and reached maximum values of 305°C and 353°C respectively.

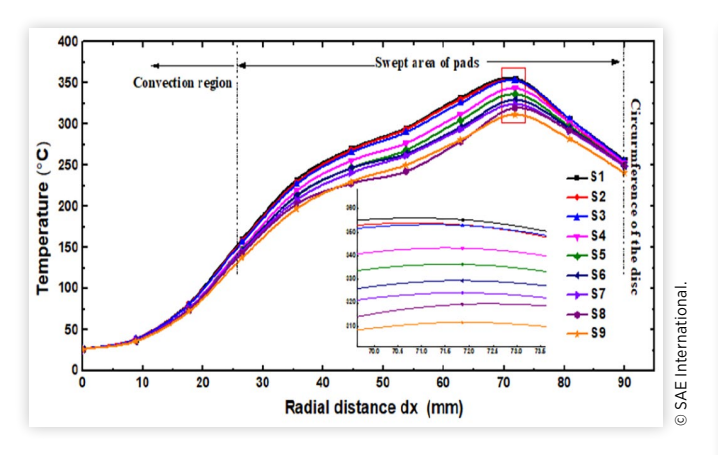
<u>Figure 9</u> depicts the radial temperature distribution on the friction ring section of the disc at certain cover angles of the pads. The temperature field distribution for all the discs

FIGURE 8 Temperature distribution through the disc rotor at 30° pad cover angles



TRANSIENT HEAT TRANSFER SIMULATION AND BUCKLING ANALYSIS OF DISC BRAKES

FIGURE 9 Distribution of temperature along the radial of the disc for different cover angles of the pads



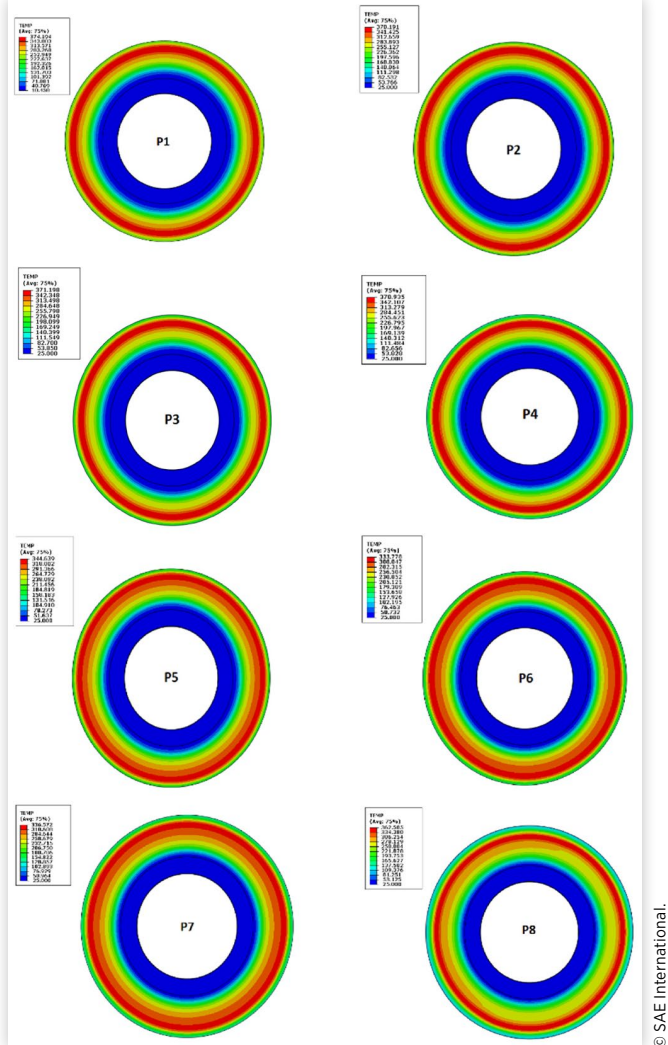
has a similar pattern along the radial direction. The highest radial temperature for each disc occurred at the same radial distance $dx = 73.0 \, mm$. This is expected because the friction work is the same. Nonetheless, peak temperature distribution values were found to be different. This behavior forms an important part of this work. The observed phenomenon can lead to some discs undergoing buckling even though the same work is considered for all braking conditions. This phenomenon was investigated and discussed in Section 4.3.

4.2. Influence of Pad Positions on Temperature Distribution

The pad positions on the disc were varied at different positions to investigate its influence on temperature field distribution. The inner and outer radius of each pad were altered such that it provided the exact positions needed to be placed on the disc rotors while maintaining the same contact area and the same friction work. It is obvious that at different positions, the braking torque will be different. Therefore, the braking time and torque required to generate the same friction force on each disc during braking were computed. The disc labeled P1, P2, P3, P4, P5, P6, P7 and P8 have corresponding pads positioned at $R_p = R_d$, $r_p = 172.1 \ mm < r < R_p = 236 \ mm$, $r_p = 170$. $8 \ mm < r < R_p = 235 \ mm, r_p = 169.4 \ mm < r < R_p = 234 \ mm,$ $r_p = 168.0 \text{ } mm < r < R_p = 233 \text{ } mm, r_p = 166.6 \text{ } mm < r < R_p = 2$ $32 \text{ mm}, r_p = 165.2 \text{ mm} < r < R_p = 231 \text{ mm}, r_p = 163.8 \text{ mm} < r$ $\langle R_p = 230 \text{ } mm \text{ } respectively. More precisely, the outer radius}$ of the pads is positioned at 0 mm, 1 mm, 2 mm, 3 mm, 4 mm, 5 mm, 6 mm and 7 mm away from the circumference of the disc respectively. The corresponding temperature field distributions on the discs from P1 to P8 are observed as shown in Fig. 10. It is more evident that the pad positions play a significant role in the temperature field distribution on the disc. Each disc exhibited a non-uniform temperature field distribution on its surface.

For P1, P2, P3 and P4 the non-uniform temperature field distribution appeared to have a similar distribution pattern but different magnitudes during the braking period. The deep red zone appeared to have a more spread area compared to

FIGURE 10 Variation of temperature field on the disc for different positions of the pads



the light red zone. This observation is because, at these positions, the temperature distribution is influenced by the sliding velocity compared to convection losses on the free surfaces of the disc. For P5, P6 and P7, the light red zone appeared to have the same radial distance as the deep red zone. This is because there is a reduction in sliding velocity along the radial direction at these positions. Meanwhile, the temperature distribution for P8 was found to be significantly different, with a highly concentrated red zone and an irregular temperature field distribution in some regions on the disc. It was noted from all the discs that the more spread and uniform the red zones, the lower the peak temperature exhibited. Figure.11 shows the variation of maximum temperature in each disc at the various pad positions with time. Heating of the disc at P1, P2, P3 and P4 rises faster at the beginning of the braking process compared to P5, P6 and P7, reaching maximum values of 374.19°C, 370.19°C, 371.20°C and 370.94°C respectively, it then turned down slightly due to convection. Furthermore, the disc labeled P6 showed the lowest rise in temperature with time compared to all the other discs during the braking process. The maximum temperature exhibited for P6 is found

FIGURE 11 Variation of maximum temperature with time at different pad positions on the disc

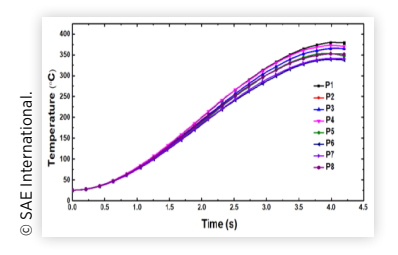
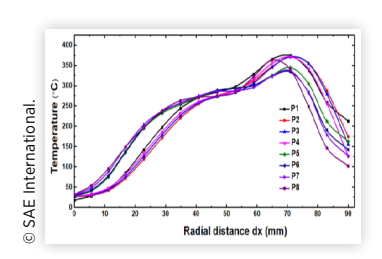


FIGURE 12 Distribution of temperature along the radial of the disc for different pad positions

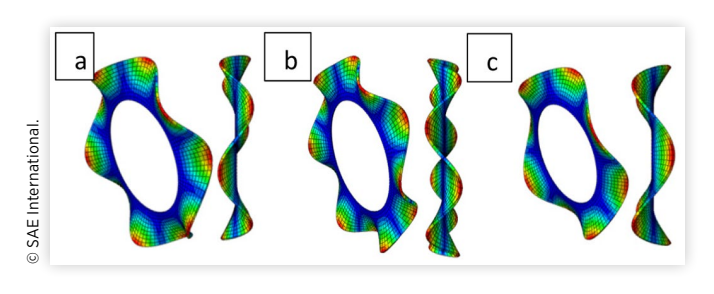


to be 333.78°C, which makes it more appropriate for the reference vehicle in terms of temperature distribution. Figure 12 depicts the temperature field distribution along the radial of the friction ring section. The radial temperature field distribution for P1, P2, P3 and P4 assumed a similar distribution profile pattern while P5, P6, P7 and P8 also assumed the same profile pattern. Nevertheless, a significant sharp rise in temperatures was observed at a radial distance ranging from $dx = 65 \, mm$ to $dx = 80 \, mm$ for P1, P2, P3 P4 and P8. The effect of this behavior on braking is investigated in Section 4.3. This phenomenon shows that, for the same work done, friction heat generated is significantly different, which may lead to thermoelastic instability [2, 16, 19].

4.3. Effects of Resulting Radial Temperature Distribution on Thermal Buckling

In this section, the eigenvalue-based buckling analysis is used to estimate the critical thermal buckling temperature of the rotor during braking. A linear perturbation procedure is used because, even if the disc has non-linearity in terms of geometry, material, etc., a general eigenvalue buckling mode can render useful information on the deformation mode. ABAQUS script was written to compute the thermal buckling mode of the rotor for the resulting radial temperature distribution during the braking period. The preloaded temperature fields (Figs. 9 & 12) applied on the friction ring section of the disc were expressed in polynomial functions of the sixthorder. The solution gives the deformation modes and the force multipliers λ_i for the temperature loads f_i defined. The force multipliers also referred to as the eigenvalues are required to compute the critical buckling temperatures. When the computed critical buckling temperature is less than the

FIGURE 13 Deformation modes for thermal Buckling a)
First-Order buckling mode b) Second-Order buckling mode c)
third-Order buckling mode



braking temperature or the applied temperature load, the rotor disc is said to have undergone deformation or buckling.

The first three deformation modes of the disc when the pads cover angles ($\theta_p = 20^\circ$) and positions $R_p = R_d$ were varied are shown in Fig. 13. The first three deformation modes for the cover angles of the pads were the same as when the pad positions were varied but with different eigenvalues or force multipliers. This could be attributed to the close-range temperature distribution in both contact geometry simulation. The corresponding eigenvalues for mode 1, mode 2 and mode 3, by varying the cover pad angles ($\theta_p = 20^\circ$) were found to be 1.007, 1.073 and 1.104 respectively while the corresponding eigenvalues for the modes by varying the pad position at $R_p = R_d$ were 1.154, 1.227 and 1.270 for modes 1, 2 and 3 respectively. The total or critical buckling temperature f_{cr} was computed by finding the product of the applied maximum temperature load and its corresponding eigenvalue or buckling load multiplier i.e. $f_{cr} = \lambda_i f$. Tables 3 & 4 show the critical thermal buckling temperatures for the first six modes when the angles and positions of the pads were varied respectively. It was observed that varying the cover angles of the pads while maintaining the same friction work have less effect on the critical thermal buckling of the disc. This result could be because the temperature field distribution differences exhibited were not so significant for each cover angle of the pad. The critical buckling temperatures were found to be higher than the braking temperature for all varied angles (θ_p) . Hence, no buckling occurred during braking by varying the cover angles. Meanwhile, at a pad cover angle of 20°, the difference in the critical temperature (357°C) and braking temperature (355.4°) was quite close. This could result in buckling of the disc during multiple braking of the vehicle.

Furthermore, considering the various position of the pads, deformation of the disc occurred at these positions $r_p = 172.1$ $mm < r < R_p = 236$ mm, $r_p = 170.8$ $mm < r < R_p = 235$ mm, $r_p = 168.0$ $mm < r < R_p = 233$ mm, $r_p = 166.6$ $mm < r < R_p = 232$ mm and $r_p = 163.8$ $mm < r < R_p = 230$ mm. At these positions, the braking temperature exceeded the critical buckling temperature. The reason for these results is due to the highly non-uniform temperature distributions from the inner to the outer radius of the disc during braking. The corresponding eigenvalues for the first deformation mode at these positions were 0.817, 0.900, 0.991, 0.873 and 0.755 respectively. This means that for an eigenvalue of 0.817 at $r_p = 172.1$ $mm < r < R_p = 236$ mm, the corresponding buckling temperature (302.4°C) is smaller than the maximum braking temperature (370.1°C).

TABLE 3 Buckling temperatures on the disc for various pad cover angles

mode	Buckling Temperature along the radial							
	20°	30°	40°	50°	60°	70°	80°	90°
1	357.9	356.2	374.9	389.9	410.8	467.1	437.6	457.5
2	381.3	379.4	399.3	415.2	437.4	496.8	465.8	486.6
3	392.3	390.4	411.1	427.8	451.0	514.3	480.7	503.3
4	434.7	432.6	455.3	473.4	498.7	566.1	531.1	554.6
5	508.6	506.2	532.9	554.2	583.9	662.8	621.9	649.5
6	-583.7	-581.2	-608.9	-631.2	-661.3	-738.0	-702.0	-725.8

TABLE 4 Buckling temperatures on the disc for various pad positions on the disc

	Buckling	Buckling Temperature along the radial							
Mode	$R_{\rho} = R_{d}$	$r_p = 172.1$ < $r < R_p = 236$	r _p = 170.8 < r < R _p = 235	r _p = 169.4 < r < R _p = 234	$r_p = 168.0$ < $r < R_p = 233$	$r_p = 166.6$ < $r < R_p = 232$	r _p = 165.2 < r < R _p = 231	$r_p = 163.8$ < $r < R_p = 230$	
1	431.7	302.7	334.1	574.8	341.5	291.5	254.1	518.0	
2	459.2	322.6	356.1	608.5	363.5	310.5	270.6	548.9	
3	474.9	331.0	365.7	637.3	374.6	319.3	277.9	573.7	
4	523.4	367.5	405.8	691.2	414.3	353.6	307.9	623.9	
5	612.9	429.3	474.6	807.1	484.7	413.3	359.3	729.0	
6	-687.5	504.9	-552.7	-875.9	-556.6	-482.5	422.0	-795.7	

Therefore, the rotor will deform at this braking temperature. The negative temperatures obtained at the sixth mode for certain positions of the pads indicate that the corresponding eigenvalues were negative and that deformation will occur when the applied temperature load direction is reversed. From the results in <u>Table 4</u>, it can be concluded that pad positions on the disc have a significant effect on the thermal buckling of the rotor during braking of the reference vehicle even by considering the same moment of friction.

5. Conclusion

In this paper, a study on the temperature field distribution of an in-wheeled-mounted disc brake component of a fully-loaded 10x10 multi-in-wheeled vehicle decelerating to a stand-still with an initial velocity of 30km/h on a flat road was presented. The effect of contact geometry on the temperature field distribution and the effect of the resulting temperature on thermal buckling during braking were investigated. The cover angle of the pads (θ_p) and the pad positions on the disc were varied. Based on the results, the following conclusions are drawn:

1. For the same friction work by different cover angles of pads on the disc during braking, the minimum temperature is reached on the disc with the largest cover angle of pad whereas the maximum temperature is reached for the disc with the smallest cover angle of pad. However, the maximum temperature difference for the disc at various cover angles is approximately equal and the temperature field distributions on the disc assumed a similar profile pattern. Besides, the resulting temperature field had no significant effect on the thermal buckling of the disc during braking.

2. Also, considering the same work done by the brake pads at different locations on the disc rotor, the maximum temperatures and temperature fields were greatly influenced during braking. Depending on the position of the pad, the peak temperatures varied on the disc surface. The temperature distribution for disc P1 where $R_p = R_d$ and P8 where $r_p = 163.8 \ mm < r < R_p = 230 \ mm$ were found to be inappropriate for the in-wheeled brake system in terms of temperature field distribution. However, at these positions and also at $r_p = 169.4 \ mm < r < R_p = 234 \ mm$ and $r_p = 165.2 \ mm < r < R_p = 231 \ mm$, thermal buckling did not occur during braking. In general, the position of pads on the disc surface has a significant effect on the thermal buckling of the disc during braking.

Acknowledgments

The present study is part of a project carried out at the University of Denver and financed by the National Science Foundation under Contract No. 1928876. We acknowledge the support from Beijing Institute of Technology (China), Vehicle Engineering Laboratory.

Reference

- 1. Liu, M., Huang, J., and Chao, M., "Multi-States Combination Nonlinear Control of In-Wheel-Motor-Drive Vehicle Dynamics Stability," *Energy Procedia* 105:2746-2752, 2017, doi:10.1016/j.egypro.2017.03.926.
- 2. Wang, J., Wang, Q., Jin, L., and Song, C., "Independent Wheel Torque Control of 4WD Electric Vehicle for

- Differential Drive Assisted Steering," *Mechatronics* 21(1):63-76, 2011, doi:10.1016/j.mechatronics.2010.08.005.
- 3. Hwang, P., Wu, X., and Jeon, Y., "Repeated Brake Temperature Analysis of Ventilated Brake Disc on the Downhill Road," 2008, https://doi.org/10.4271/2008-01-2571.
- 4. Choi, J.-H., and Lee, I., "Finite Element Analysis of Transient Thermoelastic Behaviors in Disk Brakes," *Wear* 257(1-2):47-58, 2004, doi:10.1016/j.wear.2003.07.008.
- Grzes, P., Oliferuk, W., Adamowicz, A., Kochanowski, K. et al., "The Numerical-Experimental Scheme for the Analysis of Temperature Field in a Pad-Disc Braking System of a Railway Vehicle at Single Braking," *International Communications in Heat and Mass Transfer* 75:1-6, 2016, doi:10.1016/j.icheatmasstransfer.2016.03.017.
- Ghadimi, B., Sajedi, R., and Kowsary, F., "3D Investigation of Thermal Stresses in a Locomotive Ventilated Brake Disc Based on a Conjugate Thermo-Fluid Coupling Boundary Conditions," *International Communications in Heat and Mass Transfer* 49:104-109, 2013, doi:10.1016/j. icheatmasstransfer.2013.10.009.
- Karan Dhir, D., "Thermo-Mechanical Performance of Automotive Disc Brakes," *Materials Today: Proceedings* 5(1):1864-1871, 2018, doi:10.1016/j.matpr.2017.11.287.
- 8. Belhocine, A., and Bouchetara, M., "Thermal Analysis of a Solid Brake Disc," *Applied Thermal Engineering* 32:59-67, 2012, doi:10.1016/j.applthermaleng.2011.08.029.
- 9. Chen, Z., Yi, Y.-B., Bao, K., and Zhao, J., "Numerical Analysis of the Coupling between Frictionally Excited Thermoelastic Instability and Thermal Buckling in Automotive Clutches," *Proceedings of the Institution of Mechanical Engineers, Part J: Journal of Engineering Tribology* 233(1):178-187, 2019, doi:10.1177/1350650118772664.
- 10. Yi, Y.-B., Shaahu, J.-S., and Chen, Z., *Instabilities Induced by Thermal-Mechanical Couplings in Clutch and Brake Discs* (Warrendale, PA: SAE International, 2018), https://doi.org/10.4271/2018-01-1894.
- 11. Chen, Z., Yi, Y.-B., and Zhao, J., "Fourier Finite Element Model for Prediction of Thermal Buckling in Disc Clutches and Brakes," *Journal of Thermal Stresses* 39(10):1241-1251, 2016, doi:10.1080/01495739.2016.1215728.
- 12. Vescovini, R., and Dozio, L., "Thermal Buckling Behaviour of Thin and Thick Variable-Stiffness Panels," *J. Compos. Sci.* 2(4):58, 2018, doi:10.3390/jcs2040058.
- 13. Yang, Q., Zhang, B., Ding, K., and Song, L., "Finite Element Analysis of a Brake Disc under Constant Mechanical Loading," 2017, https://doi.org/10.4271/2017-01-2490.
- 14. Anderson, A.E., and Knapp, R.A., "Hot Spotting in Automotive Friction Systems," *Wear* 135(2):319-337, 1990, doi:10.1016/0043-1648(90)90034-8.
- Meng, D., Liu, J., Zhang, J., and Zhang, L., "Study on Brake Disc Dynamics under Asymmetric Thermal Loads," SAE Technical Paper <u>2018-01-1901</u>, 2018, https://doi.org/10.4271/2018-01-1901.
- 16. Lee, K., and Barber, J.R., "Frictionally Excited Thermoelastic Instability in Automotive Disk Brakes," *Journal of Tribology* 115(4):607, 1993, doi:10.1115/1.2921683.

- McPhee, A.D., and Johnson, D.A., "Experimental Heat Transfer and Flow Analysis of a Vented Brake Rotor," *International Journal of Thermal Sciences* 47(4):458-467, 2008, doi:10.1016/j.ijthermalsci.2007.03.006.
- 18. Talati, F., and Jalalifar, S., "Analysis of Heat Conduction in a Disk Brake System," *Heat and Mass Transfer* 45(8):1047-1059, 2009, doi:10.1007/s00231-009-0476-y.
- 19. Grzes, P., "Determination of the Maximum Temperature at Single Braking from the FE Solution of Heat Dynamics of Friction and Wear System of Equations," *Numerical Heat Transfer, Part A: Applications* 71(7):737-753, 2017, doi:10.1080/10407782.2017.1308711.
- 20. Yevtushenko, A.A., Kuciej, M., Grzes, P., and Wasilewski, P., "Temperature in the Railway Disc Brake at a Repetitive Short-Term Mode of Braking," *International Communications in Heat and Mass Transfer* 84:102-109, 2017, doi:10.1016/j.icheatmasstransfer.2017.04.007.
- Mills, A.F., "Heat Transfer," Second Edition, Prentice Hall Inc., ISBN 0-13-947624-5, 1999.
- 22. Limpert, R., *Brake Design and Safety* (Warrendale, PA: SAE International, 1999), ISBN:1-56091-915-9.
- 23. Hwang, P., Wu, X., and Jeon, Y., "Repeated Brake Temperature Analysis of Ventilated Brake Disc on the Downhill Road," 2008, https://doi.org/10.4271/2008-01-2571.
- Wang, G., and Fu, R., "Impact of Brake Pad Structure on Temperature and Stress Fields of Brake Disc," Advances in Materials Science and Engineering 2013:1-9, 2013, doi:10.1155/2013/872972.
- 25. Adamowicz, A., and Grześ, P., "Convective Cooling of a Disc Brake during Single Braking," *Acta Mechanica et Automatica* 6, 2012.
- 26. Yevtushenko, A., and Grzes, P., "Finite Element Analysis of Heat Partition in a Pad/Disc Brake System," *Numerical Heat Transfer, Part A: Applications* 59(7):521-542, 2011, doi:10.108 0/10407782.2011.561098.
- 27. Grześ, P., "Numerical Analysis of Temperature Field in a Disc Brake at Different Cover Angle of the Pad," *Acta Mechanica et Automatica* 8(4):185-188, 2014, doi:10.2478/ama-2014-0033.
- 28. He, L., and Ovaert, T.C., "Heat Partitioning Coefficient Calculations for Sliding Contacts with Friction," *Tribology Transactions* 51(1):12-18, 2008, doi:10.1080/10402000701739248.
- 29. Day, A., "Thermal Effects in Friction Brakes," *Braking of Road Vehicles* (Elsevier, 2014, 215-258, doi:10.1016/B978-0-12-397314-6.00007-3.

Nomenclatures

- a_d Contact on the disc, (m^2)
- A_s Contact surface area (m^2)
- a_i Deceleration of the vehicle, (m/s^2)
- D Disc diameter, (m)
- F_z Vertical force on the wheel, (N)
- P_d Decelerating power (W)

TRANSIENT HEAT TRANSFER SIMULATION AND BUCKLING ANALYSIS OF DISC BRAKES

q(r, t) - Heat flux (W)

I - Mass moment of inertia for all rotating parts (200*kgm*²)

p - Contact pressure (MPa)

 R_w - Wheel radius, (m)

 T_a - Ambient/Initial temperature, (°C)

 T_{max} - Maximum temperature, (°C)

T - Temperature

h - Heat coefficient $(W/m^2/^{\circ}C)$

Z - Axial position

r - radius, (m)

 $(r, \theta, 0, t)$ - Cylindrical-coordinate system

v - velocity (m/s)

t - Time (*s*)

 Q_{in} - Amount of heat generated

 Q_{out} - Amount of heat dissipated

 ρ - Density (kg/m^3)

 ω_0 - Angular velocity (rad/s)

 α_t - Angular acceleration (rad/s²)

 ν - Kinematic viscosity of air (m^2/s)

 α - Thermal diffusivity (m^2/s)

K - Thermal conductivity (W/m^2 °C)

 δ_d - Thickness of the disc (*m*)

 γ - heat partition coefficient

Subscript

p, d, s - Pad, disc, surface

R, L - Right wheel, Left wheel

i, f - Initial, final

a - air

Contact Information

Yun-Bo Yi, Ph.D.

Associate Professor Mechanical & Materials Engineering University of Denver 2155 E Wesley Ave

Denver, CO 80208

Yun-Bo.Yi@du.edu

Phone: 303-871-2228